ORIGINAL ARTICLE

Parametric analysis of thermomechanical behavior of reinforced concrete slabs with different aggregates in fire

Análise paramétrica do comportamento termomecânico de lajes de concreto armado com diferentes agregados expostas ao fogo

Andreia Romero Fanton[a]
Luiz Carlos de Almeida[a]
Leandro Mouta Trautwein[a]

[a]Universidade Estadual de Campinas – UNICAMP, Departamento de Estruturas, Campinas, SP, Brasil

Abstract: Reinforced concrete structures, when subjected to fire, have their mechanical resistance reduced related to the behavioral change of the material. Many experimental and numerical research on the behavior of concrete exposed to fire have been carried out on beams and columns, with slabs being studied less frequently, mainly due to its size and consequently higher research costs. This paper carried out a numerical analysis of the thermomechanical behavior of reinforced concrete slabs exposed to fire, using finite element modeling. The parametric analysis carried out changing the aggregate type of concrete showed that when exposed to ISO834 fire curve, the displacement in the center of slab with siliceous aggregate was 47% higher than the slab with calcareous aggregate. Analyzing the crack opening, for slabs exposed to ISO834 fire curve, the first 1mm-cracks were noticed at 18min when using calcareous aggregate, while the slabs with siliceous aggregate started at 13min.

Keywords: concrete, fire, finite elements, numerical analysis, slabs.

Resumo: Estruturas de concreto armado, quando submetidas ao fogo, têm sua resistência mecânica reduzida em função da mudança de comportamento do material. Muitas pesquisas experimentais e numéricas sobre o comportamento do concreto exposto ao fogo têm sido realizadas em vigas e pilares, sendo as lajes menos estudadas, principalmente devido à sua dimensão e consequentemente maiores custos de ensaio. Este artigo realizou uma análise numérica do comportamento termomecânico de lajes de concreto armado expostas ao fogo, utilizando modelagem por elementos finitos. A análise paramétrica realizada alterando o tipo de agregado do concreto mostrou que, quando exposta à curva de incêndio ISO834, o deslocamento no centro da laje com agregado silicioso foi 47% maior do que a laje com agregado calcário. Analisando a abertura de fissuras, para as lajes expostas à curva de incêndio ISO834, as primeiras fissuras de 1mm foram notadas aos 18min quando se utilizou agregado calcário, enquanto as lajes com agregado silicioso iniciaram aos 13min.

Palavras-chave: concreto, fogo, elementos finitos, análise numérica, lajes.

1 INTRODUCTION

Fire safety has as its main goals human life safety and prevent property damage. Since fire situations in buildings can occur at any time, the importance of user safety (most important goal) and maintaining the integrity of the structure (secondary goal) become relevant. Structural integrity is required primarily in commercial buildings, as damages in this scope may paralyze economic activities.

In a building, the slabs are the structural elements that are less loaded and have higher ductility, i.e., they have larger deformation capacity. In a fire situation, slabs remain stable after the Ultimate Limit State is exceeded. However, slabs should ensure the physical integrity of the structure in terms of partitioning. If extreme deformations occur, fire sealing and fire stopping may be affected. If there is a collapse, there will be a spread of fire between the floors, the fire will be extended, and the structural damage will be higher.

The reinforced concrete (RC) slabs have the rebars in their bottom face as a guarantee of structural strength, where the thermal action has greater intensity. When they are cast-in-place, the slabs generally do not have reinforcement needed for crack width control to assure additional resistance if the main bottom reinforcement bars yield.

Recent catastrophes have intensified the search for a thorough understanding of the changes in the mechanical behavior of concrete when subjected to fire. On May 1st, 2018, the Wilton Paes de Almeida building in Sao Paulo suffered a major fire. The 24-storey building collapsed just over an hour and a half after the fire start. The National Museum of Rio de Janeiro, one of main ones in Brazil, was gutted in a fire on September 2nd, 2018. As no visitation was taking place at the time of the tragedy, there were no victims but 90% the collection was destroyed.

The Brazilian standard NBR 15200:2012 [1] allows the effects of additional efforts of thermal origin to be neglected in design. However, this consideration must consider the structural element dimension, in addition to its composition in the structure. The safety requirements of structures against fire prescribed in the standard refer to fire resistance, defined as the ability of a structural element to maintain its fundamental functioning when subjected to a standard fire [2]. Such resistance depends on the structural element's geometry, the materials used in the construction, the load intensity, and the fire exposure. The fire resistance tests of structures are carried out in the laboratory, exposing the structural elements to fire conditions, and monitoring their behavior. Numerical and analytical methods are a more economical alternative to those tests.

In a fire situation, many properties of concrete undergo significant changes: physical, chemical, or mechanical. According to Reddy and Ramaswamy [3], the mechanical properties are lost because the high temperature in cement paste removes the chemically bound water and weakens the cement mortar. In many cases, fire-exposed concrete elements may have their layers fragmented due to an explosion of the material, a phenomenon known as spalling.

According to Bažant and Oh [4], the spalling phenomenon has two main reasons. The first refers to the hypothesis that the increase in temperature leads to high water vapor pressures in the concrete pores. As a result, internal stresses increase, and spalling occurs. The second reason is related to the hypothesis that heating rapidly leads to thermal expansion, and this is controlled by the surrounding concrete. In this way, compressive stress arises that can result in the concrete crushing, causing damage to its surface layer.

The thermomechanical behavior of concrete exposed to fire is related to the cement paste properties. Aggregates constitute about 60% of the concrete volume. Concrete can have different strengths in an event of fire based on the type of aggregate: siliceous, calcareous (or carbonate), or lightweight. Calcareous concrete is composed of dolomite and limestone, while siliceous has sandstone, silica, and granite. Calcareous aggregate is essentially amorphous and softer than siliceous, and both have different cleavage. Siliceous concrete has higher thermal conductivity because of the higher level of crystallinity and its strength is smaller than the calcareous when subjected to fire.

The objective of this study is to analyze the thermomechanical behavior of RC slabs in fire through numerical modelling. Slabs were subjected to ISO834 time-temperature curve. The model was calibrated against experimental and numerical results from the literature. Two different types of aggregates were studied: calcareous and siliceous. The results provide information to understand the influence of aggregates on the thermomechanical behavior of RC slabs exposed to fire.

2 THEORETICAL BACKGROUND

2.1 Concrete properties in fire

Concrete is a heterogeneous material, and its behavior, when exposed to high temperatures (above 60°C), is of great complexity. The models to represent the properties as a temperature rise function are elaborated through average curves. These curves are established by results of experiments or numerical modeling [5]. The concrete model used is based on the fracture-plastic model. For concrete, the temperature-dependent concrete properties were based on Eurocode 2 (EN 1992-2:2004) and are presented on item 3.6.

2.1.1 Density

There is an interrelationship between density and thermal expansion. Most solid materials expand when heated, and contract when cooled, i.e., there is a change in volume that acts on the density [5]. At high temperatures, there is a

reduction in the concrete density due to the evaporation of water that is free in the material, and the increase in volume caused by thermal expansion. As shown in a review by Costa [5], in practice, the reduction in the density of normal concrete in fire is not very significant in relation to the other thermal properties. In this way, the density is independent of the temperature.

2.1.2 Thermal elongation

Due to the restrictions generated by thermal dilatation, thermal elongation (or stretching) is essential for the analysis of 2nd order effects, especially when frames are modelled. In the case of isolated elements, it can also be convenient in simplified calculation methods. The elongation is determined through the relationship between the elongation that occurs with the increase in temperature and the initial length of the element - this being at a temperature of 20°C, with restricted axial displacement [6].

2.1.3 Thermal conductivity

If there is a temperature gradient, the conduction mechanism allows heat to flow in solid media. Through Fourier's Law, the heat flux is proportional to the temperature gradient in the considered direction, multiplied by the area where the heat undergoes such transfer. Therefore, thermal conductivity is directly linked to the heat conduction capacity that the material has, in Watt per meter and degree Celsius (W/m°C) [6]. In the case of concrete, the thermal conductivity is reduced with the rise in temperature, and is related to the aggregate used, in addition to the porosity of the cement paste. Through dehydration of concrete, the tendency is that this property reduces with increasing temperature.

2.1.4 Specific heat

Specific heat is a property defined as the amount of heat required to raise the material temperature by one degree in one unit of mass. The specific heat unit is Joule per kilogram and degree Celsius (J/kg°C). The water evaporation quantification is an approximation of the mass transfer phenomenon. Similarity theory is the approach used to predict evaporation rate. It is a standard basis used to predict evaporation rate from free water surface, and states that convective heat and mass transfer are analogous phenomena under certain conditions.

There are three different functions for determining the concrete specific heat, considering that there is a constant peak value for temperatures between 100°C and 115°C, according to EN 1992-1-2:2004 [7]. The existence of this peak is related to the water evaporation that is free inside the concrete. If this water is not completely evaporated, the temperature in the microstructure of the concrete will be limited to grow up to 100°C. Variations in the simulated moisture value can significantly change the response of the models.

2.2 Concrete mechanical properties

Anderberg and Thelandersson [8] proposed the concrete constitutive law for high temperature conditions in transient regimes, according to the experiments performed. For the formulation to be as adequate as possible, the total strain is given as the sum of four different parcels, each related to a different test, as follows:
• thermal strain: including shrinkage, measured on unstressed specimens under variable temperature;
• instantaneous stress-related strain: based on stress-strain curves obtained under constant temperature;
• creep-strain: time-dependent strain, measured under constant temperature;
• transient strain: responsible for the increase temperature effect under stress, obtained from tests under constant stress and variable temperature.

The law can be expressed as follows:

$$\varepsilon_T = \varepsilon_{th}(T) + \varepsilon_\sigma(\tilde{\sigma}, \sigma, T) + \varepsilon_{cr}(\sigma, T, t) + \varepsilon_{tr}(\sigma, T) \tag{1}$$

where ε_T = total strain (%); ε_{th} = thermal strain (%); ε_σ = stress-related strain (%); ε_{cr} = creep strain (%); ε_{tr} = transient strain (%); T = temperature; σ = stress (kN/cm^2); $\tilde{\sigma}$ = stress history (kN/cm^2); and t = time (s).

A detailed description of each parcel can be found in Fanton [9]. The modulus of elasticity (Ec), critical compressive displacement (Wd), plastic strain at peak compressive stress (εcp), fc' and εth coefficients were considered multiplied to the initial value of the parameters at normal temperatures and are shown on item 3.6.

3 NONLINEAR NUMERICAL MODELLING

Nonlinear finite element analyses (NLFEA) are a useful tool to investigate and predict the behavior of reinforced concrete structures. Here, the heat transfer analysis implemented in ATENA is applied to study the slab behavior. A brief review of previous fire studies using numerical research in ATENA is included to improve the discussion of the results presented in this paper.

3.1 Existing data on RC structures in fire modelled in ATENA

The ATENA software was used to study RC structures in a fire situation by:

• Cervenka et al. [10], for a three-dimensional analysis of a tunnel fire. The paper describes the modifications to the combined fracture-plastic model developed previously by the authors. The model was extended to facilitate its applicability for the simulation of reinforced concrete structures subjected to fire.

• Zlámal et al. [11] to verify the behavior of experimentally tested panels with Carbon-Glass Fibre Reinforced Polymers (CGFRP) reinforcement under effect of fire. Mathematical models were created to verify the behavior of experimentally tested panels and to provide basic data for following detailed mathematical models to predict the behavior of other FRP reinforced structures under fire effect.

• Papanikolaou and Kappos [12] for a nonlinear analysis of unreinforced concrete tunnel linings. Various modelling techniques are described, considering the plane finite element representation of the lining geometry, material constitutive laws, and boundary and interface conditions. Furthermore, all relevant external loading cases are studied, including gravity, environmental, fire, blast, and seismic loading. Potential pitfalls in the modelling and analysis procedures are identified and properly dealt with.

• Al-Kamaki [13], for a study of the strengthening of fire-damaged RC columns using CFRP fabrics. The study is extended to cylinders damaged by heating and subsequently repaired using CFRP fabrics while the cylinders were still under load or without load. An innovative technique using photogrammetry principles is used for axial and lateral strain measurement, in addition to conventional strain gauges on the surfaces of all tested columns. Finite element models were also developed using ATENA-GiD software to provide a better understanding of the behavior of both unheated and heat-damaged unwrapped or CFRP-wrapped RC columns, and to estimate the load-carrying capacity of the repaired columns.

• Blesak et al. [14] to study unprotected timber-fibre RC slab in fire.

• Jadooe et al. [15], for a study of the strengthening of heat-damaged RC beams using near-surface mounted Carbon Fiber Reinforced Polymers (NSM CFRP). Although the ultimate load and stiffness decreased, repair with near-surface mounted systems to the CFRP laminate using an epoxy- or cement-based adhesive in grooves cut into the concrete surface was found to increase the load capacity and stiffness of the beams.

• Jadooe et al. [16], to model near-surface mounted Carbon Fiber Reinforced Polymers (NSM CFRP) strips embedded in concrete after exposure to elevated temperature using epoxy adhesives. The finite element models showed reasonable agreement with the experimental results and can be used to predict the effects of high temperature on pull-out values after exposure to elevated temperatures.

• Juliafad et al. [17], for an analysis of after fire RC beam strengthened with Carbon Fiber Strip (CFS). This research obtained nonlinear Finite Element numerical model for Reinforced Concrete Beam after-fire and then strengthened with CFS on the flexural area. RC beam before the fire, after fire and strengthened after FEM model were compared with the actual experimental results.

• Sadaghian and Farzam [18], to the analyses of punching shear of RC slabs exposed to fire. Results showed that there is a slight difference in temperature endurance of various models with respect to concrete with different compressive strengths. It was also concluded that compared to a slab without gypsum, 10-mm and 20-mm thick gypsum reduce the maximum heat transferred to the slab by 45.8% and 70%, respectively.

• Fanton [9], to the analyses of the thermomechanical behavior of RC slabs exposed to fire. The numerical thermal and thermomechanical models in finite elements were calibrated from the results of experimental tests obtained in the literature. The calibration results of the models obtained were satisfactory. The parametric analysis carried out by changing the concrete aggregates showed that the behavior of concrete with calcareous aggregate is better when compared to siliceous aggregate.

Rev. IBRACON Estrut. Mater., vol. 17, no. 5, e17507, 2024

4/19

3.2 Nonlinear finite element analysis of RC structures

3.2.1 Constitutive models

The ATENA program (Advanced Tool for Engineering Nonlinear Analysis) is based on the Finite Element Method and was developed by the company Cervenka Consulting, located in the Czech Republic, and focused on numerical analysis of concrete structures. The GiD preprocessor allows the construction of model geometry, the definition of material properties, load conditions and its history by defining finite element intervals and meshes, in order to perform static analysis and heat conduction calculations (transport analysis). The models of these two analyzes are not identical, but compatible. The finite element mesh is different, but the temperatures for the static analysis are inferred from the temperatures associated with the mesh used in the thermal analysis. Figure 1 presents the nonlinear analysis composition technique using the Finite Element Method.

For brittle materials, such as concrete, ATENA uses a fracture-plastic constitutive model called Fracture-Plastic Constitutive Model which combines fracture in tension with plasticity in compression. Concrete fracture is based on the classical formulation of the smeared crack [20] and the crack band model [4]. Crack propagation is based on the theory of nonlinear fracture mechanics, through the crack opening law associated with a cohesive model.
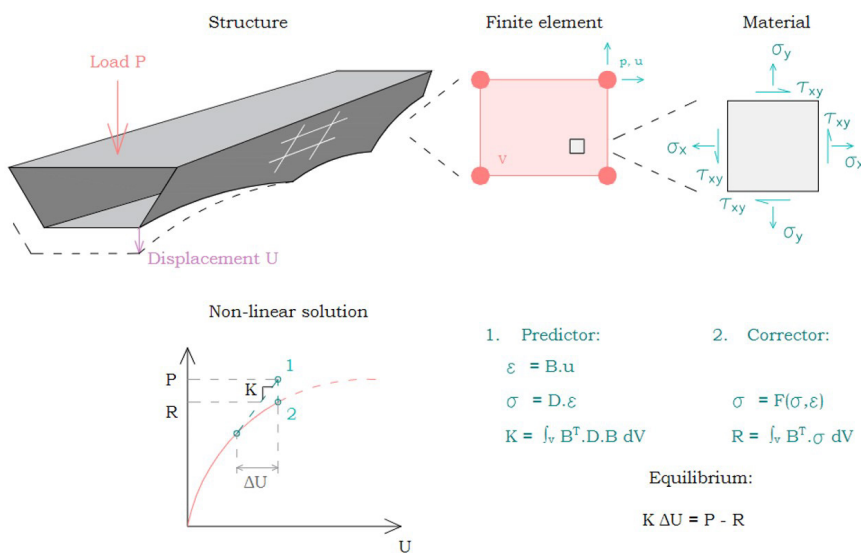

Figure 1. Non-linear analysis technique Representation through the Finite Element Method. Adapted from Pukl et al. [19]

For the material model Concrete EC2-CC3DNonLinCementitious 2, this law is given by the Hordijk [21] softening function presented in Figure 2a, where σ is the tensile stress, w is the crack opening, f_t^{ef} is the effective tensile stress and w_c is the crack opening value when $\sigma = 0$.
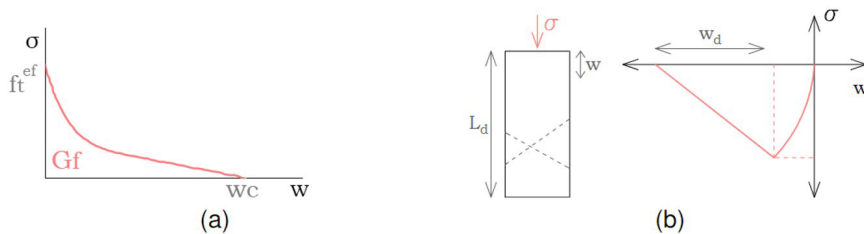

Figure 2. a) Plastic cohesive law with exponential softening in tension; b) Compressive stress-strain diagram describing concrete behavior in compression.

The compressive behaviour of concrete is determined by a Hardening/Softening Plasticity Model based on Menetrey-William [22] failure surface and is represented in ATENA by Fictitious Compression Plane Model [23]. The uniaxial stress-strain law has a linear descending branch, where the value of post-peak plastic displacement due to compression (wd) is an input parameter. For normal concrete, the value of wd is around 0,5mm and it is used as a default for the definition of the softening in compression (Figure 2b).

The reinforcement was modelled using the material model CCReinforcement, which follows stress–strain relationship by the multilinear law and is presented in Figure 3. In the model, the last eps value defines the breaking strain for the reinforcement bar. It was used eps2 as 0.005, f1 as 560 MPa and f2 as 588 MPa.
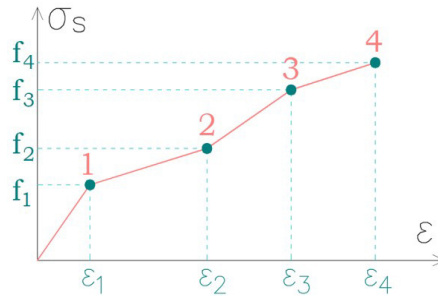
Figure 3. The multi-linear stress-strain law for reinforcement

3.3 Numerical modelling

The Finite Element model was calibrated against experimental and numerical results conducted by Ali et al. [24]. The slabs were simply supported concrete slabs 3300x1200x200 mm with an average concrete cube strength of 42 MPa at 28 days. Each slab was reinforced with 6ϕ12mm longitudinal steel bars (T12 in Figure 4) and 13ϕ10mm secondary reinforcement steel bars (T10 in Figure 4). The concrete cover was 40mm vertically and 50mm on slab sides. They were subjected to conventional ISO834 time-temperature curve with a clear span of 3000mm, 3 slabs. The temperatures were measured at three depths: surface, 40mm (steel reinforcement), and 100mm. All slabs were tested under 0,65 (including self-weight) (27kN) of the design load of BS8110 (1997) applied at the mid-span point of the slab. The numerical analysis performed by Ali et al. [24] used DIANA software. The concrete slab body was modelled using a 3D twenty-node solid brick element. As the moisture migration phenomenon and vapor pressure build up in concrete have high complexity nature, these phenomena are not considered in the model.

The concrete slabs were modeled using the Finite Element Method based software tools GiD 10.0.9 (pre-processing) and ATENA 5.6.1 (processing and post-processing). ATENA (Advanced Tool for Engineering Nonlinear Analysis) is an advanced engineering tool capable of simulating the real behavior of concrete. GiD generates relevant input, finite element meshes and enables a range of calculation options as variable loading, temperature, and time inputs to be run by ATENA. After geometry creation, material properties are defined and assigned to volumes in the model.

Figure 4 shows the geometry of the concrete slab modelled. In assembling the model within GiD, the concrete slab was modelled as volume elements, and the steel reinforcement bars were added as line entities.
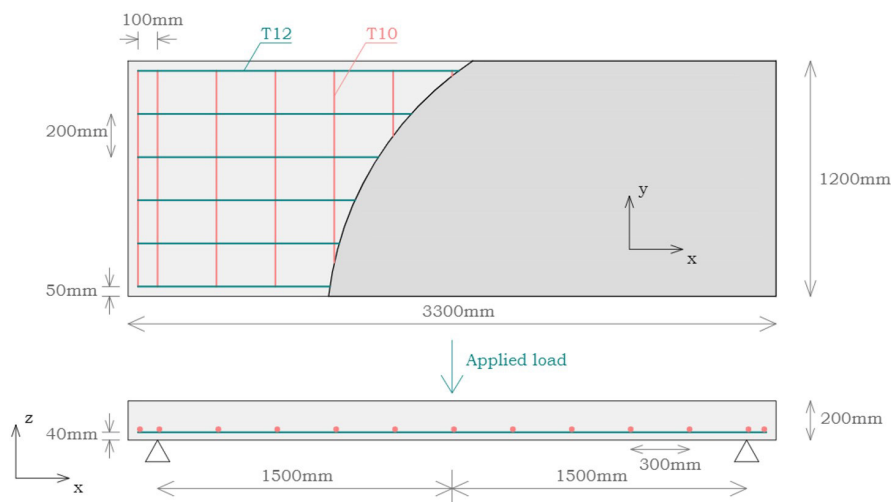
Figure 4. Geometry, loading and reinforcement details of concrete slab

The finite element used to represent concrete in the model was the CCIsoBrick20 3D (Figure 5a). This is an isoparametric element integrated by Gauss integration at integration points. Interpolation functions for all variants of the

elements are given in Cervenka et al. [23]. The constant part of initial moisture value considered on the numerical model was 0,9728. The finite element used to represent the reinforcement in the model was the CCBarWithBond 3D (Figure 5b).

The calibration is performed in three steps, as follows: **step I**: mechanical behavior of the slab under normal conditions at room temperature; **step II**: thermal behavior of the slab in fire situation; **step III**: thermomechanical behavior of the slab in a fire situation.
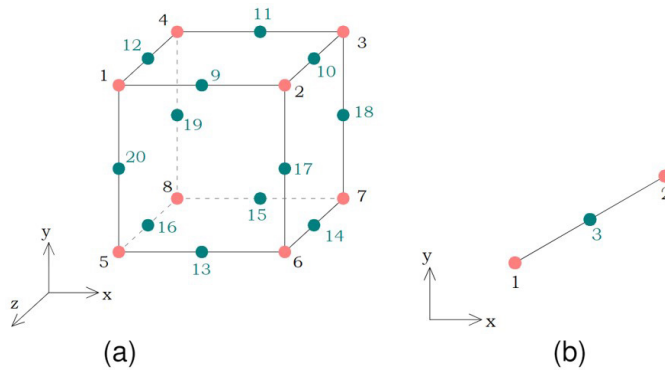

(a)   (b)

Figure 5. a) CCIsoBrick20-3D b) CCBarWithBond-3D

3.4 Calibration step I: mechanical behavior

In this step, only the dead load and applied load were considered. Figure 6 shows the numerical model of the slab. A mesh sensitivity study was not done in this study once the same mesh criteria from Ali et al. [24] was used to compare the models.
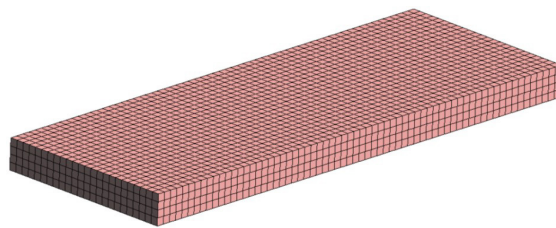

Figure 6. Slab model

To allow loading in mid-span, the slab was equally divided into 4 volumes (Figure 7).
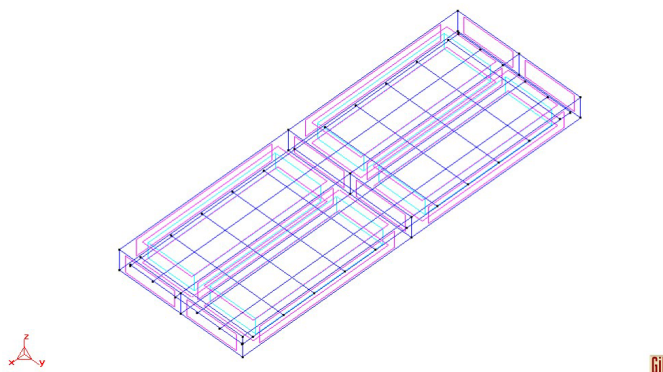

Figure 7. Slab division

As boundary conditions (Figure 8), considering the slab as simply supported and static, line constraints were applied to restrict the vertical movement (z-axis) in the bottom edges and the longitudinal movement (x-axis) in the central bottom edge of the slab.
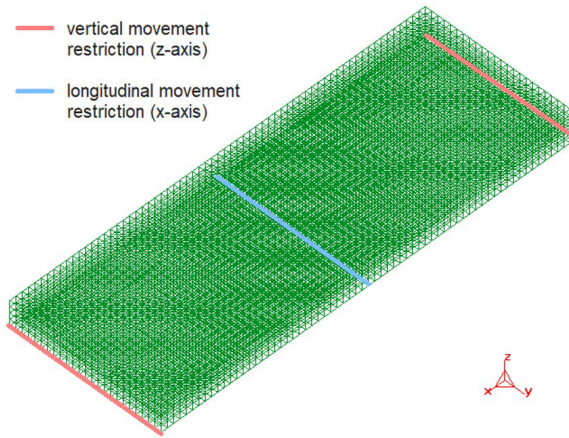
Figure 8. Slab boundary conditions

The equations were solved using Newton-Raphson method. The iteration limit was defined as 20. The meshed model consisted of 31422 nodes. Table 1 (based on Ali et al. [24]) shows the mechanical properties of the model elements, where fc' is the compressive strength, ft is the tensile strength, fy is yield strength, fu is the ultimate strength and E is the Young's modulus.

Table 1. Material properties.

	Concrete	Steel
fc' [MPa]	42	-
ft [MPa]	2,52	-
fy [MPa]	-	534,8
fu [MPa]	-	669,2
E [MPa]	39,3	209

The mechanical parameters of plastic deformation of the concrete (εcp) and the compressive strength at the beginning of the non-linear behavior ($f'c0$) were calculated according to the equations:

$$\varepsilon_{cp} = \frac{f_{cm}}{E_{cm}} \tag{2}$$

$$f'_{c0} = 2 \cdot f_{cm} \tag{3}$$

The other parameters were used as the program default values and are presented in Table 2.

Table 2. Concrete parameters – constitutive model.

	Initial value	Adjusted value
E_{cm} [MPa]	39000	39300
ν	0,2	0,2
f_{tm} [MPa]	2,07	2,07
f_{cm} [MPa]	-40	-40
G_f [N/m]	51,7	51,7
Aggregate size [m]	0,02	0,02
s_F	1	1
ε_{cp}	-0,0015636	-0,0015636
f'_{c0} [MPa]	-4,34	-4,34
w_d [m]	-0,0005	-0,0005
$f_{c,red}$	0,8	0,8
e	0,52	0,52
β	0	0

where E_{cm} = modulus of elasticity of the concrete; ν = Poisson coefficient; f_{tm} = direct tensile strength; f_{cm} = resistance to cylindrical compression; G_f = concrete fracture energy; s_F = shear factor; $\mathcal{E}_{cp}$ = plastic deformation of concrete; f'_{c0} = compressive strength of concrete at the beginning of the non-linear regime; w_d = post-peak plastic displacement due to compression; $f_{c,red}$ = reduction factor of concrete compressive strength; e = dimensionless eccentricity parameter; β = shear retention factor.

Other properties were defined as: processor type = 64-bit; number of threads = -2; solution method = Newton-Raphson; stiffness type = Elastic Predictor; stiffness matrix = at each step; solver = LU; iteration limit = 20.

3.5 Calibration step II: thermal behavior

To analyze the thermal behavior, only the thermal loads (time-temperature curves) were considered, using the same slab geometry. Heat transfer analysis was performed for the concrete slab body. The interval time was assumed as 3600 seconds. The condition *Fire boundary for surface* was used to apply fire loading to the bottom surface, simulating the conventional ISO834 time-temperature curve shown in Figure 9. It was directly applied to the surface using FIRE CURVE ETK (represented by ISO 834 curve in Figure 9). The convection heat transfer coefficient used was 25 W/°C·m^2 (as in Ali et al. [24]). The resulting emissivity factor of the radiation source and heat transfer used was 0,7.
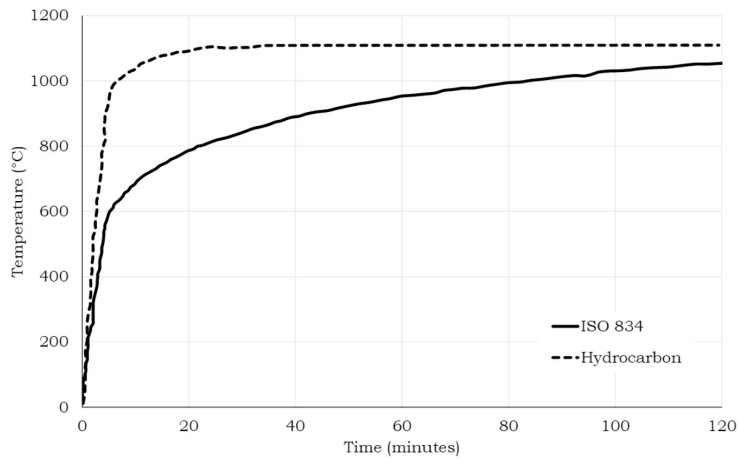

Figure 9. ISO834 and hydrocarbon time-temperature curves. Adapted from Eurocode 2 (EN 1992-2:2004).

The meshed model consisted of 31369 nodes. Concrete was modelled as CCTransport Material, with the properties shown in Table 3. The initial values are the ATENA default parameters available. The adjusted values presented in Table 3 are the values used on the numerical model, according to the experimental data (Ali et al. [24]).

Table 3. CCTransport Material parameters.

		Initial value	Adjusted value
Thermal conductivity	[W/°C·m]	2,1	1,1
Thermal capacitance	[kN/m^2·°C]	2550	2550
Initial temperature	[°C]	25	20
Moisture	[MPa]	0,9728	0,9728
Emissivity	[-]	-	0,7

The moisture content also measured before and after the experimental tests on both of the top and the bottom surfaces of each slab using Tramex CRH concrete moisture content measuring device. The moisture value considered on the numerical model was 0,9728 MPa.

3.6 Calibration step III: thermomechanical behavior

The *CC3DNonLinCementitous2* concrete model used is based on the fracture-plastic model. For concrete, the temperature-dependent concrete properties [thermal conductivity (kc - W/m°C), specific heat capacity (ρc), density (ρ), compressive strength (fc') and thermal expansion strain (εth)] were based on Eurocode 2 (EN 1992-2:2004). The modulus of elasticity (Ec), critical compressive displacement (Wd), plastic strain at peak compressive stress (εcp), fc' and εth coefficients were considered multiplied to the initial value of the parameters at normal temperatures and are shown in Figures 10a-d.

(a) Young's modulus.

(b) Critical compressive displacement.

(c) Thermal strain.

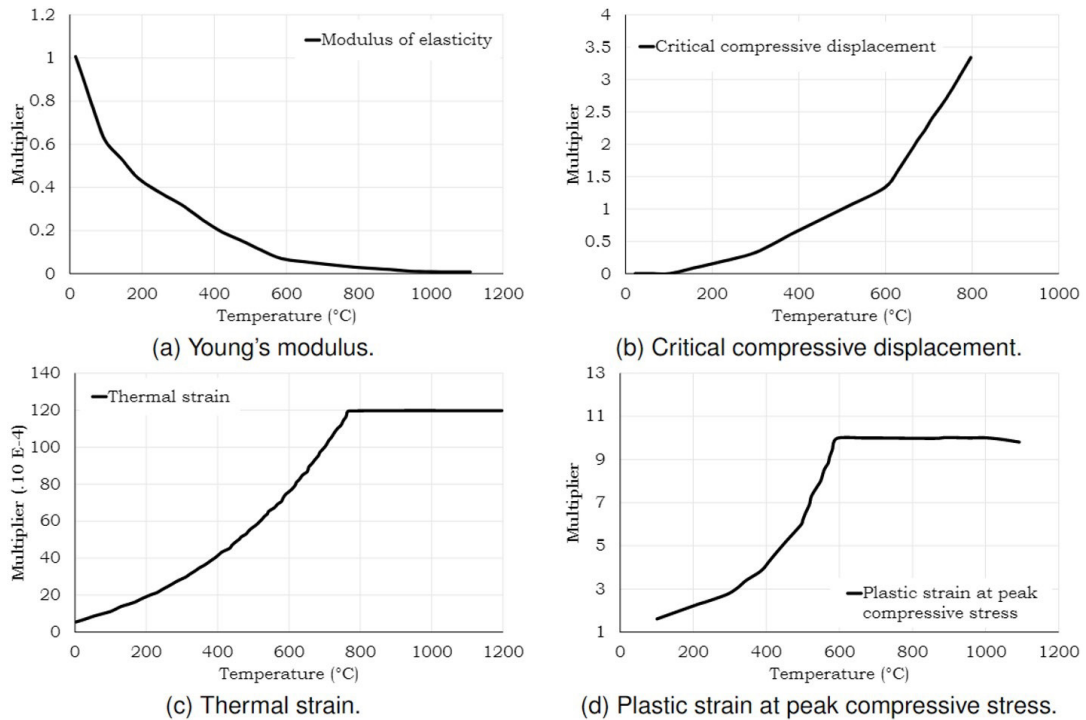(d) Plastic strain at peak compressive stress.

Figure 10. Concrete properties (Adapted from Sadaghian and Farzam [18]).

Step III consists of a study of thermomechanical slab behavior in fire situation, considering its dead load, applied load and thermal load (time-temperature curves). In this step, the thermal model data (from step II) were imported into the static model (step I). Concrete was modelled as *CC3DNonLinCementitious2WithTempDepProperties*, with calcareous aggregate, and reinforcement bars as *CCReinforcementWithTempDepProperties*.

All concrete properties can be inserted into ATENA software. When defining the solid material, for Concrete as *CC3DNonLinCementitious2WithTempDepProperties*, the equations for temperature dependence are inserted, as shown in Figure 11.

3.7 Parametric analysis

When subjected to extreme high temperature conditions, the applied type of aggregate can develop a significant impact on concrete resistance. Due to this, a parametric analysis was carried out changing the concrete aggregate. Two different aggregates are available in ATENA software: calcareous and siliceous. Their properties were duly considered in the input data. Concrete thermal expansion is influenced by the type of aggregate because of the large differences in the thermal properties of various types of aggregates. 70 to over 80 percent of the total solid volume of the concrete come from aggregates. Figure 12 shows the variation of relative compressive strength of concrete (fc) with siliceous and calcareous aggregates under elevated temperature (θ). It can be defined by Eurocode 2 [7].
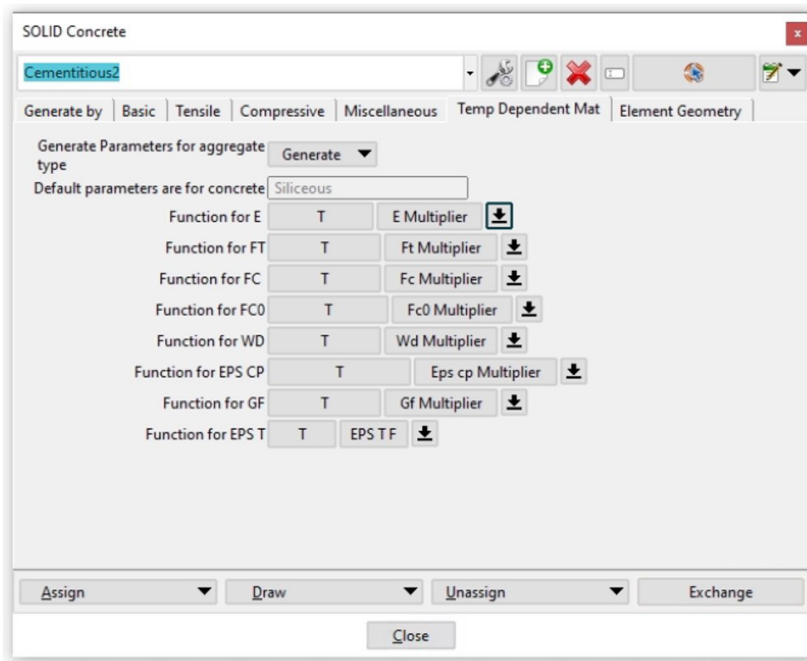
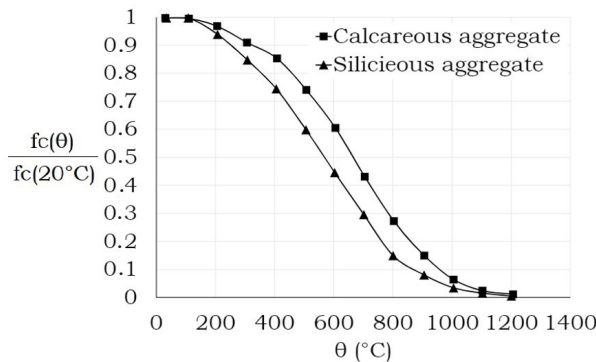**Figure 11.** Temperature dependent material – ATENA software.

Figure 12. Relative compressive strength of concrete with siliceous and calcareous aggregates at elevated temperatures. Adapted from Bacinskas et al. [25].

Siliceous aggregates have thermal coefficients of expansion between 2.5 and 3.6 millionths per degree Celsius, while calcareous aggregates vary between 0.7 and 2.5 millionths per degree Celsius. Also, the residual compressive strength of the concrete tends to increase as the thermal strain of the aggregate decreased.

The expansion is determined through the relationship between the elongation that occurs with increasing temperature and the initial length of the element - this being at a temperature of 20°C, with restricted axial displacement. The following equations show the variation in thermal expansion ($\varepsilon = \Delta L/L$) as a function of temperature.

Silicious aggregate concrete:
• $20°C \leq \theta_{conc} \leq 700°C$:

$$\varepsilon_{conc} = 9 \cdot 10^{-6} \cdot \theta_{conc} + 2{,}3 \cdot 10^{-11} \cdot \theta_{conc}^3 - 1{,}8 \cdot 10^{-4} \tag{4}$$

• $700°C < \theta_{conc} \leq 1200°C$:

$$\varepsilon_{conc} = 1{,}4 \cdot 10^{-2} \tag{5}$$

Calcareous aggregate concrete:

• 20°C ≤ θ_{conc} ≤ 805°C:

$$\varepsilon_{conc} = 6 \cdot 10^{-6} \cdot \theta_{conc} + 1{,}4 \cdot 10^{-11} \cdot \theta_{conc}^3 - 1{,}2 \cdot 10^{-4} \tag{6}$$

• 805°C < θ_{conc} ≤ 1200°C:
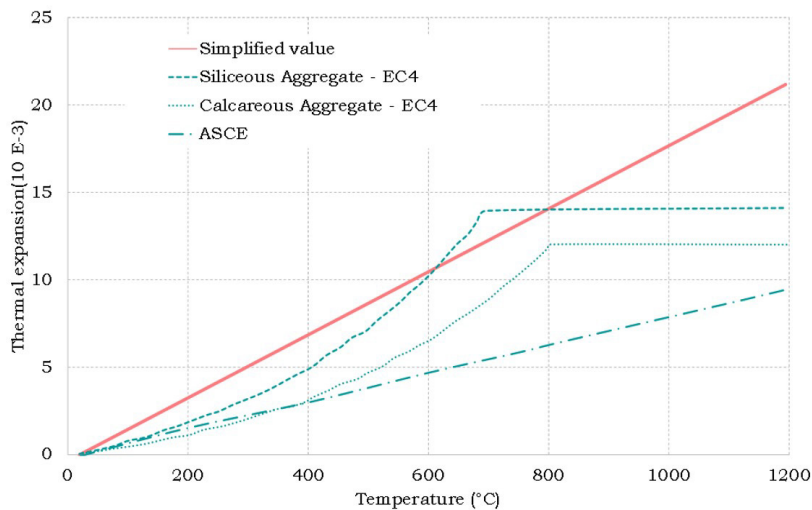
$$\varepsilon_{conc} = 1{,}2 \cdot 10^{-2} \tag{7}$$

Figure 13. Thermal expansion of concrete with siliceous and calcareous aggregates at elevated temperatures
(Adapted from Fanton [9])

In the case of simplified calculation models, a single linear function is adopted between the thermal expansion and temperature.

• 20°C < θ_{conc} ≤ 1200°C:

$$\varepsilon_{conc} = 18 \cdot 10^{-6} \cdot (\theta_{conc} - 20) \tag{8}$$

The concrete thermal expansion models most widely used are the ASCE and the Eurocode, for calcareous and siliceous aggregates. ASCE model is indicated in Equation 9 while Euro code-4 models for siliceous and carbonate aggregate concrete are indicated in Equations 4 to 7. Both models (ASCE and Euro code-4) are clearly indicated in Figure 13.

$$\varepsilon_{conc} = (4 \cdot 10^{-3} \cdot \theta_{conc}^2 + 6 \cdot \theta_{conc} - 121{,}6) \cdot 10^{-6} \tag{9}$$

The cracking pattern was not validated with experimental results since it was not presented by the authors. To make it possible to calibrate the model, thermal deformation was analyzed. The determination of stress-related strain is based on the concept that, at each stage, there is a valid stress-strain relationship for the material. This relationship represents the response of the material to a change in stress. The influence of temperature on stress-strain relationships is shown in Figure 14.
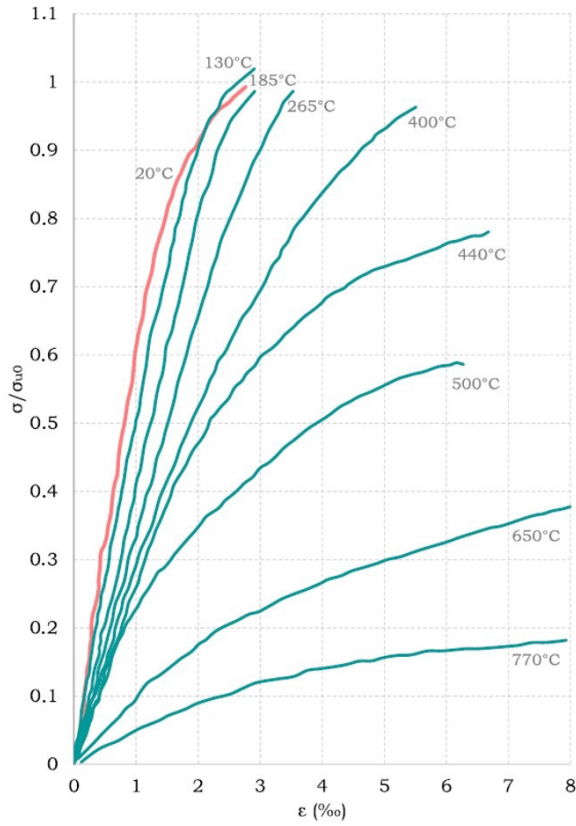
Rev. IBRACON Estrut. Mater., vol. 17, no. 5, e17507, 2024

12/19

Figure 14. Stress-strain relationships for different temperatures (Adapted from Fanton [9])

The stress-strain relationship at a given moment depends on the temperature at the time of analysis and the previous history of stresses, and its general form is shown in Figure 15.
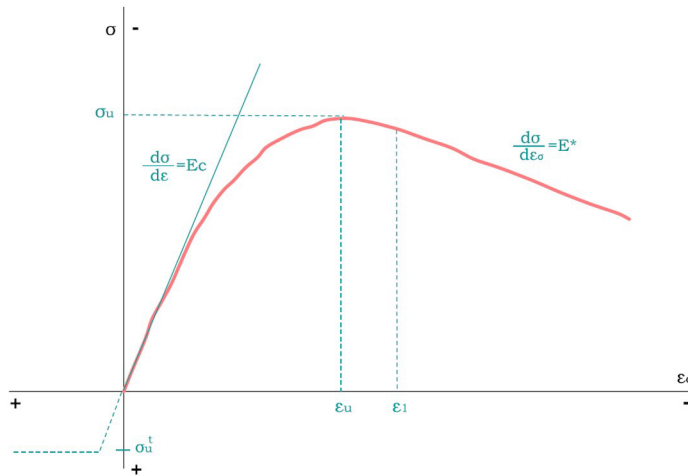

Figure 15. General description of the stress versus strain relationship (Adapted from Fanton [9])

The boundary conditions of the parabolic curve in Figure 15 are:

$\sigma = 0$ when $\varepsilon\sigma = 0$;

$\sigma = \sigma u$ when $\varepsilon\sigma = \varepsilon u$;

$\delta\sigma/\delta\varepsilon\sigma = 0$ when $\varepsilon\sigma = \varepsilon u$;

where:

σu = ultimate stress at temperature t;

εu = strain at ultimate stress.

So, for $\varepsilon\sigma$ varying between 0 and $\varepsilon 1$:

$$\varepsilon_{conc} = (4 \cdot 10^{-3} \cdot \theta_{conc}^2 + 6 \cdot \theta_{conc} - 121,6) \cdot 10^{-6} \tag{10}$$

where $\varepsilon 1$ is the deformation in the transition between the parabolic and linear descent regime.

The fictitious initial modulus of elasticity Ec, which occurs when strain ε tends to zero, is given by:

$$E_c = 2 \cdot \frac{\sigma_u}{\varepsilon_u} \tag{11}$$

When $\varepsilon 1 > \varepsilon\sigma$,

$$\sigma = E * \cdot \varepsilon_\sigma + \sigma * \tag{12}$$

where:

$$\sigma *= \sigma_u \cdot \left(1 - \frac{E*}{E_c}\right)^2 \tag{13}$$

The transition point $\varepsilon 1$ is obtained by the following equation:

$$\varepsilon_1 = \left(1 - \frac{E*}{E_c}\right) \cdot \varepsilon_u \tag{14}$$

where:

E* = slope of the descending branch;

σ* = additional stress in the descending branch.

Therefore, the stress-strain relationship depends on knowing the parameters σu, εu and E*, which must be expressed as a function of temperature and stress history.

4 RESULTS AND DISCUSSION

4.1 Validation: mechanical model

After defining the model geometry, the load ranges, the contour and applied loads, mesh generation and application of material properties, the model was processed using the *ATENA Static* function. In this step, only the static behavior of the slab is analyzed; temperature considerations are not done. Figure 16 shows the deformations on the z axis (vertical) in the slab for mechanical behavior, in the longitudinal direction.
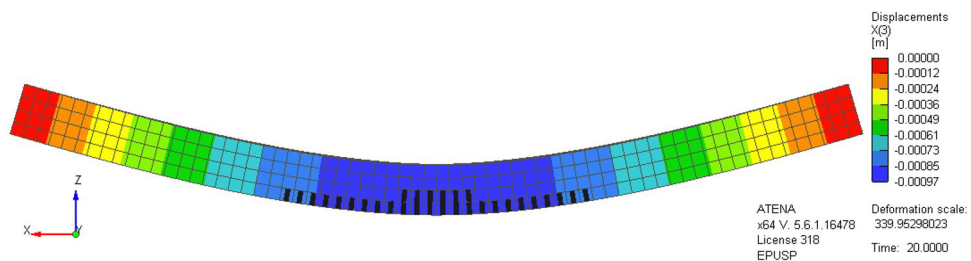

Figure 16. Displacement results and crack pattern – static analysis

Rev. IBRACON Estrut. Mater., vol. 17, no. 5, e17507, 2024

14/19

4.2 Validation: thermal model

Figure 17 shows the temperature at the slabs bottom surface exposed to ISO834 time-temperature curve. MEF Ali (2011) and Experimental Ali (2011) represent the FE results and the experimental data obtained by Ali et al. (2011). MEF ATENA presents the FE results obtained by this research.

Analyzing Figure 17, both FEM curves showed less intense temperatures during the first 10 minutes of test comparing to experimental data. This can be caused by furnace calibration during the experiment. From 14 minutes until the end of the test, the FE data of this study showed good agreement with experimental curve.

The difference between FEM ATENA and experimental data can be caused by different calibration of the numerical models. In this paper, the calibration was done against time-temperature and displacement curves. Ali et al. [24] don't explain their calibration method.
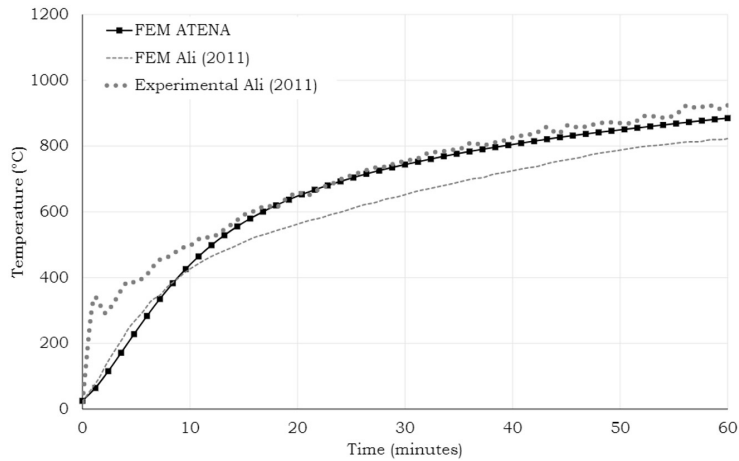

Figure 17. Temperatures at slab bottom surface - ISO834 time-temperature curve

Another possible point of divergence between the numerical and experimental results is the performance of the experimental test. In this case, small inaccuracies in calibrating the furnace, supplying energy for its operation, or measuring temperatures through thermocouples can lead to results that do not match expectations.

4.3 Validation: thermomechanical model

For ISO834 time-temperature curve analysis, the displacements at the slab center in FEM analysis showed good agreement with experimental results from Ali et al. [24] (Figure 18). At 60 minutes, the difference observed was 10,4% between FEM ATENA and Experimental Ali (2011) results, against 15,7% between FEM Ali (2011) and Experimental Ali (2011). Maximum vertical displacement observed was 36,2mm (Figure 19). These values can provide a representative validation.
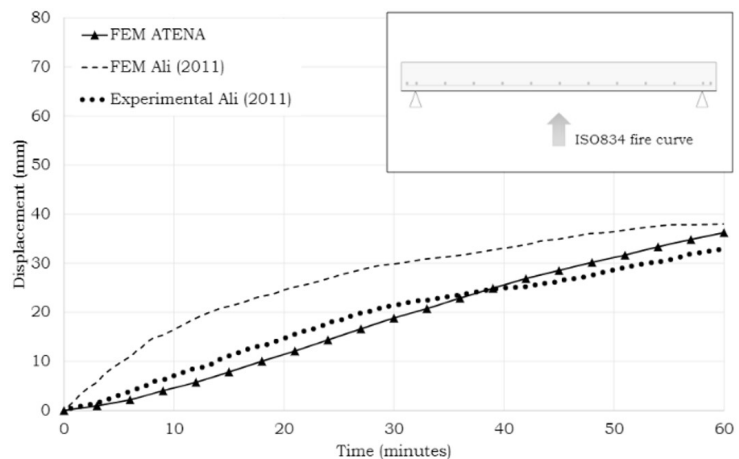

Figure 18. Displacements at slab center - ISO834 time-temperature curve

Figure 19. Displacement results and crack pattern - ISO834 time-temperature curve

4.4 Parametric analysis

Figure 20 shows the displacement at the center of the slab for ISO834 time-temperature curve. FEM ATENA - Calcareous represents the displacement for slabs with calcareous aggregate and FEM ATENA - Siliceous for siliceous aggregate. The slab behavior was better for calcareous aggregate concrete as the displacement in siliceous model was 47% bigger than calcareous.
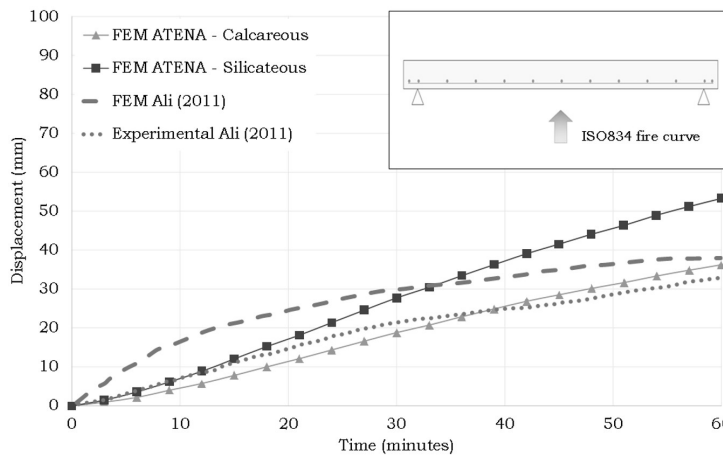

Figure 20. Displacement at the center of the slab – Parametric analysis (calcareous and siliceous aggregate) – ISO834 time-temperature curve

4.4.1 Cracking beginning

During the exposition to fire, the concrete cracking occurs due to the tensile strength exceeding, caused by thermal expansion and dehydration. When concrete surface cracking happens, pathways for direct reinforcement bars heating can occur, bringing more thermal stress. The crack width is calculated by multiplying the crack spacing by the crack inducing strain. EN 1992-1-1 shows that:

$$w_k = s_{r,máx} \cdot \varepsilon_{cr} \tag{15}$$

where $s_{r,máx}$ maximum crack spacing; ε_{cr} = creep strain (%).

Analyzing both calcareous and siliceous models, exposed to ISO834 time-temperature curve, it is possible to compare the difference between their cracking beginning moment. The slabs with calcareous aggregate presented the first 1mm-cracks at 18min, while the slabs with siliceous aggregate started at 13min.

Figure 21 shows the values of crack width for ISO834 time-temperature curve. FEM ATENA - Calcareous represents the displacement for slabs with calcareous aggregate and FEM ATENA - Siliceous for siliceous aggregate.

Comparing the numerical values obtained by FEM ATENA for calcareous and siliceous aggregate, it can be concluded that siliceous aggregate slabs presented a maximum crack width of 3.85mm, and 2.31mm for calcareous aggregate. The difference between both aggregates were expected, following the variation of relative compressive strength of concrete presented in Figure 12. Experimentally obtained mechanical and thermal properties of materials could accurate the results.
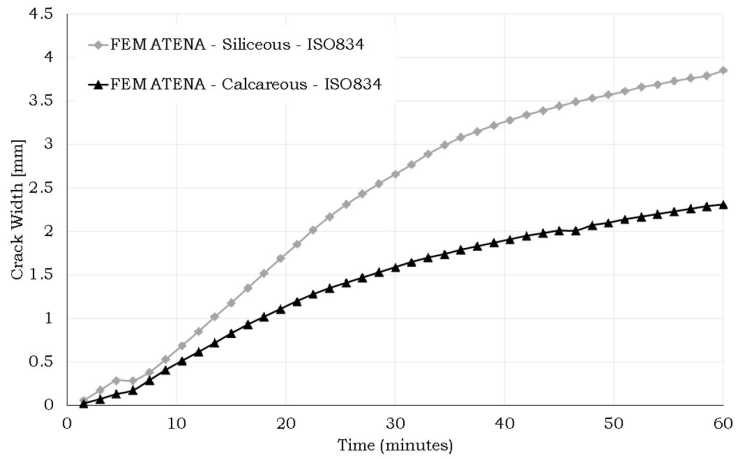
Figure 21. Crack width – Parametric analysis (calcareous and siliceous aggregate) – ISO834 time-temperature curve

4.4.2 Cracking pattern

Comparing both calcareous and siliceous models, it was possible to analyze the difference on cracking pattern. Figures 22 and 23 show the crack pattern at the slabs bottom surface exposed to ISO834 time-temperature curve, with calcareous and silicious aggregate, respectively. For ISO834 time-temperature curve exposition, siliceous aggregate slabs presented a maximum crack width of 3.85mm, and 2.31mm for calcareous aggregate slabs.
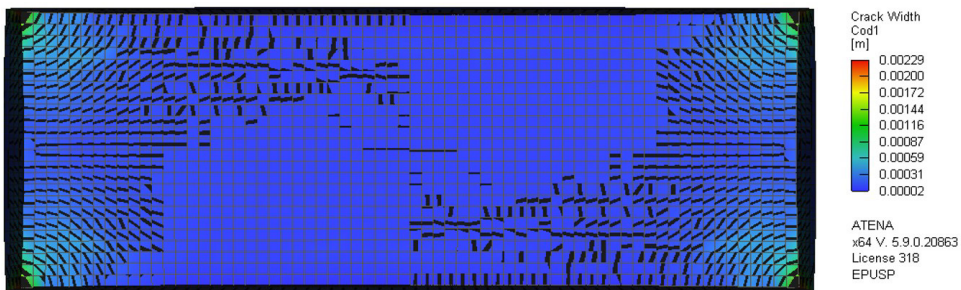

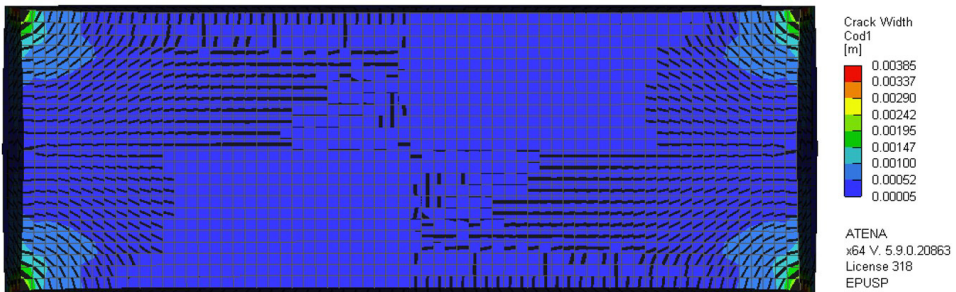**Figure 22.** Crack pattern (calcareous aggregate) – ISO834 time-temperature curve

Figure 23. Crack pattern (siliceous aggregate) – ISO834 time-temperature curve

Regarding the ISO834 time-temperature curve exposition, siliceous aggregate slabs presented 66.67% bigger crack widths than calcareous aggregate slabs.

5 CONCLUSIONS

By comparing the results obtained by the thermal model and by the thermomechanical model, it can be concluded that the structure behavior was well represented. The time-temperature curves variation applied to the slab showed the concrete behavior under different heat intensities. The slabs were subjected to ISO834 time-temperature curves.

The fire resistance of reinforced concrete structures influences the chosen materials which are used in the concrete. This influence can be positive or negative. The parametric analysis carried out in this study provided information related to different thermomechanical behavior of concrete with calcareous and siliceous aggregate exposed to fire. The second one developed worse behavior in both time-temperature curves analyzed. For ISO834 curve, the vertical displacement in the slab center with siliceous aggregate was 47% bigger than the one with calcareous.

It was concluded that the crack pattern starts at the corners and go to the center. Regarding the ISO834 time-temperature curve exposition, siliceous aggregate slabs presented a maximum crack width of 3.85mm, and 2.31mm for calcareous aggregate.

The main contribution of the parametric analysis was in filling a niche gap in crack behavior of slabs in fire since the different aggregate analysis with full description of the parameters is not frequently presented in literature. The evaluation of the effect of aggregate on parameters main contribution was to provide insight on which aggregate should be chosen so that the fire design could be optimized.

With the definition of the cracking pattern for each of the different types of aggregates, the basis for the future development of a model for predetermining the spalling behavior of slabs exposed to fire is provided.

A moderate increment in crack beginning was obtained by using siliceous aggregate instead of calcareous aggregate, for both fire-curve exposures. It was noticed that the fire behavior of the slabs with siliceous aggregate appeared more ductile. Slabs with siliceous aggregate presented good improvements in cracking while developing larger deflections than the slabs with calcareous aggregate.

ACKNOWLEDGEMENTS

REFERENCES

[1] Associação Brasileira de Normas Técnicas, *Projeto de Estruturas de Concreto em Situação de Incêndio*, ABNT NBR 15200, 2012.

[2] A. Levesque, "Fire performance of reinforced concrete slabs," M.S. thesis, Worcester Polytech. Inst., 2006, 196 p. [Online]. Available: https://web.wpi.edu/Pubs/ETD/Available/etd-042806-171420/unrestricted/ALevesque.pdf

[3] D. H. Reddy and A. Ramaswamy, "Influence of mineral admixtures and aggregates on properties of different concretes under high temperature conditions I: experimental study," *J. Build. Eng.*, vol. 14, pp. 103–114, 2017, http://dx.doi.org/10.1016/j.jobe.2017.09.013.

[4] Z. P. Bažant and B. H. Oh, "Crack band theory for fracture of concrete," *Mater. Constr.*, vol. 16, no. 3, pp. 155–177, 1983, http://dx.doi.org/10.1007/BF02486267.

[5] C. N. Costa, "Dimensionamento de elementos de concreto armado em situação de incêndio," Ph.D. dissertation, Univ. São Paulo, São Paulo, Brazil, 2008 (in Portuguese). [Online]. Available: https://www.teses.usp.br/teses/disponiveis/3/3144/tde-04092008-155911/pt-br.php

[6] D. P. Maximiano, "Análise numérica avançada de estruturas de aço e de concreto armado em situação de incêndio," Ph.D. dissertation, Univ. Fed. Ouro Preto, Ouro Preto, Brazil, 2018 (in Portuguese). [Online]. Available: https://www.repositorio.ufop.br/bitstream/123456789/10033/1/TESE_An%C3%A1liseNum%C3%A9ricaAvan%C3%A7ada.pdf

[7] European Committee for Standardization, *Eurocode 2 - Design of Concrete Structures – Part 1-2: General Rules – Structural Fire Design*, EN 1992-1-2, 2004.

[8] Y. Anderberg, S. Thelandersson, *Stress and Deformation Characteristics of Concrete at High Temperatures 2. Experimental Investigation and Material Behaviour Model* (Bulletin of Division of Structural Mechanics and Concrete Construction 54). Lund: Lund Institute of Technology, 1976, p. 86.

[9] A. R. Fanton, "Análise numérica do comportamento termomecânico de lajes de concreto armado expostas ao fogo," Ph.D. dissertation, Univ. Est. Campinas, Campinas, Brazil, 2019 (in Portuguese). [Online]. Available: https://doi.org/10.47749/T/UNICAMP.2019.1101303

[10] J. Cervenka, J. Surovec, and P. Kabele, "Modelling of reinforced concrete structures subjected to fire," *Comput. Model. Concr. Struct.*, vol. 1, pp. 1–8, 2006, http://dx.doi.org/10.1201/9781003060680.

[11] M. Zlámal, A. Kucerová, and P. Stepánk, "Effect of fire on FRP reinforced concrete structures," in *Proc. Centr. Eur. Towards Sustainable Build. Low-Tech High-Tech Mater. Technol. Sustainable Build.*, 2013, vol. 13, no. 13, pp. 1–9.

[12] V. K. Papanikolaou and A. J. Kappos, "Practical nonlinear analysis of unreinforced concrete tunnel linings," *Tunn. Undergr. Space Technol.*, vol. 40, pp. 127–140, 2014, http://dx.doi.org/10.1016/j.tust.2013.09.016.

[13] Y. S. S. Al-Kamaki, "strengthening of fire-damaged RC columns using CFRP fabrics," Ph.D. dissertation, Fac. Sc., Eng. Tech., Swinburne Univ. Technol., Melbourne, Australia, 2015. [Online]. Available: https://researchbank.swinburne.edu.au/file/8d445121-8c96-4110-827b-13b5b0a8bc56/1/Yaman%20Sami%20Shareef%20Al-Kamaki%20Thesis.pdf

[14] L. Blesak, E. Caldova, and F. Wald, "Unprotected timber-fibre reinforced concrete slab in fire," *Wood Res.*, vol. 4, no. 60, pp. 605–616, 2015.

[15] A. Jadooe, R. Al-Mahaidi, and K. Abdouka, "Experimental and numerical study of strengthening of heat-damaged RC beams using NSM CFRP strips," *Constr. Build. Mater.*, vol. 1, no. 154, pp. 899–913, 2017, http://dx.doi.org/10.1016/j.conbuildmat.2017.07.202.

[16] A. Jadooe, R. Al-Mahaidi, and K. Abdouka, "Modelling of NSM CFRP strips embedded in concrete after exposure to elevated temperature using epoxy adhesives," *Constr. Build. Mater.*, vol. 1, no. 148, pp. 155–166, 2017, http://dx.doi.org/10.1016/j.conbuildmat.2017.05.027.

[17] E. Juliafad et al., "Nonlinear finite element method analysis of after fire reinforced concrete beam strengthened with carbon fiber strip", in *Proc. 1st Int. Conf. Adv. Sci. Innovation*, 2017, pp. 1–8, https://doi.org/10.1088/1742-6596/1175/1/012019.

[18] H. Sadaghian and M. Farzam, "Numerical investigation on punching shear of RC slabs exposed to fire," *Comput. Concr.*, vol. 23, no. 3, pp. 217–233, 2019, http://dx.doi.org/10.12989/cac.2019.23.3.217.

[19] R. Pukl et al. , "Performance of fibre reinforced concrete structures-modelling of damage and reliability," *Key Eng. Mater. Trans Tech Publications*, vol. 711, pp. 690–697, 2016.

[20] Y. R. Rashid, "Ultimate strength analysis of prestressed concrete pressure vessels," *Nucl. Eng. Des.*, vol. 7, no. 4, pp. 334–344, 1968, http://dx.doi.org/10.1016/0029-5493(68)90066-6.

[21] D. Hordijk, "Local approach to fatigue of concrete," Ph.D. dissertation, Delft Univ. Technol., Delft, The Netherlands, 1991.

[22] P. Menetrey and K. J. William, "Triaxial failure criterion for concrete and its generalization," *ACI Struct. J.*, vol. 36, pp. 311–318, 1995, http://dx.doi.org/10.14359/1132.

[23] V. Cervenka, L. Jendele, and J. Cervenka, *ATENA Program Documentation, Part 1: Theory*, Prague, Czech Republic: Cervenka Consult., 2017.

[24] F. Ali, A. Nadjai, and A. Abu-Tair, "Explosive spalling of normal strength concrete slabs subjected to severe fire," *Mater. Struct.*, vol. 44, pp. 943–956, 2011, https://doi.org/10.1617/s11527-010-9678-5.

[25] D. Bacinkas et al., "Computationally effective tool for mechanical simulation of reinforced concrete members subjected to fire," in *Proc. 9th Int. Conf. Modern Buil. Mater. Struct. Tech.*, 2007, pp. 461–467.

Rev. IBRACON Estrut. Mater., vol. 17, no. 5, e17507, 2024

19/19